Arctic catastrophes in an idealized sea ice model

Ian Eisenman

March 15, 2007

Abstract

With recent observations of diminishing summer Arctic sea ice extent, the hypothesis of a "tipping point" in summer ice cover has been the focus of a number of studies. This view suggests that as summer Arctic sea ice cover retreats it will reach a critical point after which the ice–albedo effect will cause the summer ice cover to disappear altogether. We have examined the heuristic argument behind this hypothesis using an idealized, but observationally constrained, model of Arctic sea ice with representations of ice and ocean mixed layer thermodynamics, varying open water fraction, an energy balance atmosphere, and scalable CO_2. We find that summer ice cover retreats toward an ice-free summer ocean at an accelerating rate in a scenario with exponentially increasing CO_2. However, we find no critical CO_2 concentration or "tipping point" using observationally based parameter values. We identify in the extended parameter space a bifurcation associated with multiple summer ice cover states and a cusp catastrophe, and we find that it occurs far from the physically realistic parameter regime. Our results suggest that the argument for a "tipping point" in summer Arctic ice cover brought on by ice albedo may not hold up when quantified. The reason is related to the fact that ice cover has only just begun to retreat at the time of maximum sunlight (June), and the minimum ice area occurs in September when there is very little Arctic sunlight.

1 Introduction

The retreat of summer sea ice cover in the Arctic is one of the most dramatic signals of recent climate change. While winter ice cover has remained fairly constant, summer ice extent has diminished significantly during the past few decades (Fig. 1), with annual minimum extent shrinking by 20% between 1979 and 2005 [34]. The high sensitivity of Arctic sea ice cover is believed to be related to the difference in albedo (i.e., reflectiveness) between sea ice and the open water that is exposed when it melts. Bare or snow-covered sea ice reflects most sunlight back to space, while the dark ocean surface absorbs most incident light. Global climate models have long predicted reduced Arctic sea ice cover as an amplified response to global warming (e.g., Manabe and Stouffer [15]), prompting speculation more than a decade ago about the use of Arctic ice observations to provide an early indicator of climate change [35].

I. Eisenman, 2007. Arctic catastrophes in an idealized sea ice model. In 2006 Program of Studies: Ice (Geophysical Fluid Dynamics Program), pp. 131-161. Woods Hole Oceanog. Inst. Tech. Rept. 2007-02.

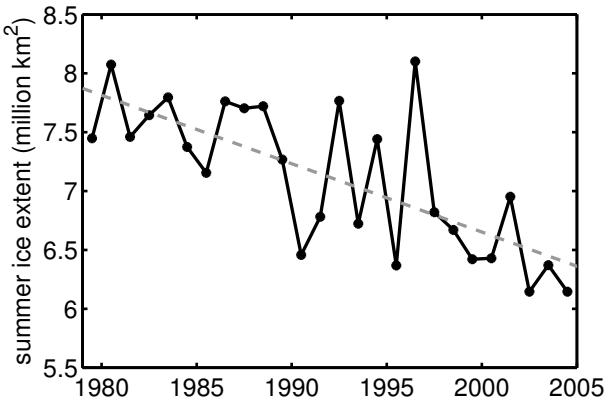

Figure 1: Diminishing Northern Hemisphere summer sea ice extent based on satellite observations [3]. Ice extent is defined as the area of grid boxes with ice concentration of at least 15%, and September monthly mean values are plotted (note that September is the month of minimum ice cover). The gray dashed line indicates a linear fit.

The ice–albedo effect could potentially lead to multiple states, and scientists have long conjectured that the Arctic might support a second stable state under current climate forcing which is at least seasonally ice-free (e.g., Ewing and Donn [5]). Heuristically, one might indeed expect that ice-free and ice-covered stable states could exist, separated by an unstable state in which the Arctic is partially covered by ice and absorbs just enough sunlight to maintain the ice edge at the freezing temperature: adding a slight amount of additional ice to this intermediate state would lead to less solar absorption, cooling, and hence further expanded ice cover. As the background climate is warmed, the unstable state would require more and more ice so that it reflects enough sunlight for the ice edge to remain at the freezing temperature. This warming could be caused by rising greenhouse gas levels, for example, or by some mechanism leading to increased heat transport into the Arctic. At a particular level of warming, the background climate would become so hot that the Arctic ocean would remain above the freezing point even if it were fully covered with ice. At this point the stable ice-covered state and unstable intermediate state would merge and disappear in a saddle-node bifurcation, leaving only the ice-free state. This scenario suggests that if the Arctic were in the ice-covered state and climate were warmed beyond the bifurcation point, it would make a rapid and irreversible transition to the ice-free state, exhibiting behavior which is described mathematically as a catastrophe.

In light of the continued recent retreat of summer Arctic sea ice cover [29], the idea that we may be approaching a threshold has been receiving a tremendous amount of attention in the popular press. Often employing the term made popular by the title of Malcolm Gladwell's bestselling sociological treatise *The Tipping Point* (2000), widespread speculations have suggested that the ice–albedo effect may cause an otherwise gradual global warming to pass a point of no return, beyond which the Arctic would rapidly approach a state which is ice-free each summer. The cover of the 3 April 2006 issue of *Time Magazine* suggests in large bold letters: "Be Worried. Be Very Worried.... Earth at the tipping point." Diminishing Arctic sea ice is a major focus of the cover story. A news feature in *Nature* on 15

June 2006 titled "The tipping point of the iceberg" discusses the increasing interest in the idea of tipping points in the climate system. The article states that among several plausible tipping points under discussion, Arctic sea ice has received the most recent attention. It reports that 234 newspaper articles mentioned a tipping point in connection with climate change during the first five months of 2006, a stark increase from 45 such articles in 2004.

In the scientific literature, discussions about a bifurcation point in summer sea ice are slightly less abundant, but several recent papers speculate about it. Lindsay and Zhang [14] write, "The late 1980s and early 1990s could be considered a tipping point during which the ice-ocean system began to enter a new era of thinning ice and increasing summer open water because of positive feedbacks. It remains to be seen if this era will persist.... However, at this point we can only state the tipping point as a hypothesis." This is based on forcing an ice-ocean model with atmospheric observations and finding significantly increased heat absorption since the 1980s associated with ice albedo; they do not actually look for hysteresis. Overpeck et al [25] conclude that the arctic appears to be heading on "a trajectory to a new, seasonally ice-free state" because of the ice–albedo feedback. They add, "The processes and interactions among primary components of the Arctic system, as presently understood, cannot reverse the observed trends toward significant reductions in ice", implying that the system has passed a bifurcation point and ice will continue to decrease until it arrives at a new state. Serreze and Francis [28] speculate about similar bifurcation behavior: "We are likely near the threshold when absorption of solar radiation during summer limits ice growth the following autumn and winter, initiating a feedback leading to a substantial increase in Arctic Ocean surface air temperatures." These papers do not actually claim that there is a "tipping point". Rather, they express it as a hypothesis and discuss its plausibility.

It is not at all obvious, however, that the ice–albedo effect would lead to multiple Arctic sea ice states and hence allow for the possibility of a catastrophe. There are many stabilizing feedbacks in the Arctic climate system. Perhaps the most important of these in the context of sea ice is the fact that thin ice grows considerably more rapidly than thick ice. For example, Untersteiner [33] gives an annual increase in thickness of 0.8m for ice that is 0.6m thick at the start of the growing season, but an increase of only 0.2m for ice that is initially 2.2m thick. Furthermore, if there were a second stable state that is at least seasonally ice-free, it would seem likely that both states would have been explored by the climate system in the past during the significant variability associated with glacial cycles. But most paleoclimate reconstructions suggest that there was year-round Arctic sea ice for at least the past million years (e.g., Moran et al [21]).

In this project, we have attempted to quantitatively investigate the plausibility of a catastrophe in summer Arctic sea ice cover. One possible approach for such an inquiry would be to employ the sophisticated global climate models which are used to predict future climate change. As described in Section 2, however, these models disagree markedly in their simulations of Arctic sea ice changes in a warming climate. Instead, we have approached the problem by constructing an idealized model of the coupled Arctic ice-ocean-atmosphere system. The model is physically stripped down to essentials, but it is observationally constrained and includes all the ingredients in the heuristic argument for multiple summer ice cover states brought on by the ice–albedo effect. To that extent, a positive result would imply only the plausibility of a "tipping point", but a negative result provides a somewhat

stronger refutation. The model is described in Section 3. It is an extension of the Arctic sea ice and atmosphere model of Thorndike [31] with additions to allow for partial ice cover, an ocean mixed layer which is always active, a simple parameterization of ice dynamics, scalable CO_2, and a change in the treatment of atmospheric heat transport which is expected to be more realistic in climate states that may be very different from today. The model is represented by four coupled ordinary differential equations that evolve ice volume, ice area, ice surface temperature, and ocean mixed layer temperature. These equations have thresholds at the freezing temperature for the ice surface and ocean mixed layer, as well as a threshold in the evolution of ice area associated with whether the ice volume is decaying.

The model results are described in Section 4. We begin by examining the model solution in the parameter regime representing the climate today. We find only one sea ice state, in contrast to the "tipping point" hypothesis. An exponential increase in CO_2 leads to retreating summer ice cover at an accelerating rate. When CO_2 is increased somewhat beyond the point where the ocean becomes ice-free each summer, the Arctic continues to be completely ice-covered every winter. When CO_2 is further increased, however, this seasonally ice-covered state gives way to a state which is ice-free year-round. Only at this point do multiple states exist: for a range of CO_2 values, both seasonal ice cover and ice-free year-round states are possible, leading to a fold catastrophe in winter ice cover as CO_2 is varied.

This suggests that the stabilizing effect of the growth-thickness relation may quantitatively outweigh the ice–albedo effect. To quantify the extent to which the former dominates in this model, we explore the parameter space in search of a region with multiple summer ice cover states. We find such a region, bounded by a saddle-node bifurcation of cycles, when we significantly reduce the latent heat of sea ice fusion. An investigation of the cusp catastrophe in CO_2–latent heat parameter space reveals that the actual Arctic appears to be far from the region where CO_2 changes can cause a "tipping point" in summer sea ice cover.

Concluding remarks and caveats regarding limitations of the idealized model are discussed in Section 5.

2 Arctic sea ice changes predicted by global climate models

Sophisticated global climate models (GCMs) have been used extensively to predict future climate change associated with increasing levels of atmospheric CO_2. About two dozen of these models are being evaluated for the incipient Fourth Assessment Report (AR4) of the Intergovernmental Panel on Climate Change (IPCC). The models typically have horizontal resolutions of 1° to 4° in the ocean component and similar equivalent spectral resolutions in the atmospheric component; the atmosphere and ocean components each typically have 10 to 50 vertical layers. All of the GCMs include representations of sea ice, with varying levels of complexity in the sea ice models.

A possible approach to address the plausibility of a catastrophe in summer Arctic sea ice cover would be to increase CO_2 in one of these GCMs, continue the simulation until the model is sufficiently spun up, and then decrease CO_2 and look for hysteresis in the ice cover. This hysteresis would imply a bifurcation or "tipping point". The simulation would be rather computationally intensive, as it would likely take more than 1000 simulation years

to sufficiently reach a steady state for the elevated CO_2 value.

The first 100 years of a similar experiment has already been evaluated with many of these GCMs for the Special Report on Emission Scenarios (SRES) A1B scenario, which is one of the CO_2 future emission scenarios investigated in the IPCC AR4. The IPCC AR4 Model Output Database at the Lawrence Livermore National Laboratory Program for Climate Model Diagnosis and Intercomparison currently has ice cover data for the "Climate of the 20th Century" and "SRES A1B" experiments from 16 of the models. We acquired the monthly gridded data from Run 1 for each of these experiments and computed the time series of total Northern Hemisphere sea ice extent by summing the area of grid boxes with ice concentration greater than 15%. The 16 models are as follows: BCCR BCM2 (Norway), CGCM3.1 T47 (Canada), CGCM3.1 T63 (Canada), CNRM CM3 (France), CSIRO Mk3 (Australia), ECHAM5 (Germany), GISS AOM (United States), GISS ER (United States), HadCM3 (United Kingdom), HadGEM1 (United Kingdom), INM CM3 (Russia), IPSL CM4 (France), MIROC3.2 low resolution (Japan), MIROC3.2 high resolution (Japan), MRI CGCM 2.3.2a (Japan), and NCAR CCSM3.0 (United States).

The average seasonal cycle in Northern Hemisphere ice extent during 1980-1999 for each of the 16 models is plotted in the top panel of Fig. 2. Ice extent during the same period computed from ice concentration measurements derived by Cavalieri et al [3] from satellite observations is included for comparison. The agreement between models and observations is decent (cf. Parkinson et al [26]): observed ice extent varies between 6 and 16 million km^2 during the seasonal cycle, and the intermodel spread is roughly ± 3 million km^2 (although it is slightly greater than this during summer).

Predicted Northern Hemisphere summer minimum sea ice extent during 2000-2100 for the "SRES A1B" experiment varies widely between the models. While the MIROC3.2 high resolution model simulates an ice-free summer Arctic starting in 2030, GISS ER simulates that in 2100 summer ice cover will be reduced by only 15%. The other models fill the space of predictions in between. In should be noted that these GCMs show better agreement in their predictions of future global mean temperatures, which is the result typically receiving the most attention. This formidable intermodel spread in simulated ice cover discourages the use of GCMs to assess the possibility of a future catastrophe in Arctic sea ice cover. It motivates an approach using an idealized model with more transparent physics, which is the method pursued in this report.

In a related project carried out this summer (Eisenman, Untersteiner, and Wettlaufer, *in prep*), we used an idealized model to examine the possibility that the spread in IPCC AR4 sea ice predictions is related to the sea ice models in the GCMs having been tuned to simulate observationally reasonable ice cover today, despite a large spread in simulated Arctic cloudiness which would otherwise lead to widely differing simulated present ice cover. The detailed results of the project have been left out of this report for brevity.

3 Model description

Here the idealized model of the coupled Arctic sea ice, ocean, and atmosphere used in this project is described. It is an extension of the model of Thorndike ([31], hereafter T92), which is a single-column model with representations of vertical sea ice thermodynamics and a thermal radiative balance atmosphere. When the ice melts to zero thickness in

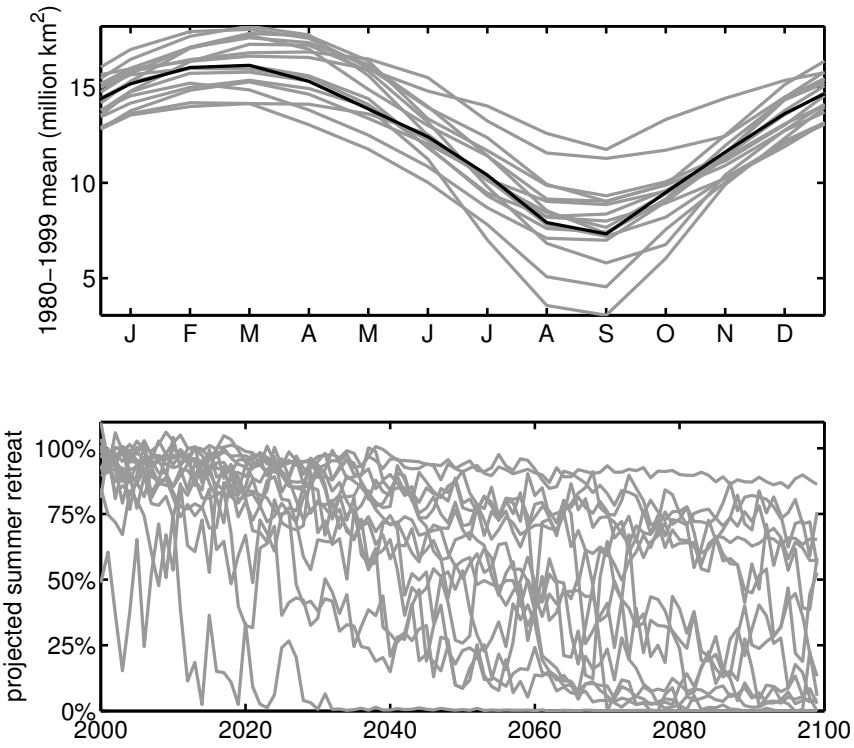

Figure 2: Simulated Northern Hemisphere sea ice extent in 16 IPCC AR4 GCMs. (Top panel) Average seasonal cycle during 1980-1999 from "Climate of the 20th Century" experiment. Ice extent derived from satellite observations during the same period is indicated by a black line. Note the decent agreement between models and observations. (Bottom panel) Predicted decrease in annual minimum monthly mean ice extent during 2000-2100 from "SRES A1B" experiment. Minimum extent is plotted for each model as a percent of the minimum in the 1980-1999 mean seasonal cycle. The intermodel spread is formidable, discouraging the use of GCMs to assess the possibility of a future ice catastrophe and motivating the use of an idealized model.

Thorndike's model, a thermodynamic ocean mixed layer is evolved until it reaches the freezing temperature, at which point sea ice begins to form again. Thorndike's model displays two stable states. One is state ice-covered year-round and the other is ice-free year-round. A third state also exists with seasonal ice cover, but it is unstable.

The model used here is extended to allow partial ice cover, which requires an ocean mixed layer which is always in communication with the atmosphere unless the ocean is completely ice-covered. The ice area is evolved using a methodology based on Hibler [10]. A simple parameterization of ice dynamics is included. The atmosphere used here is nearly identical to Thorndike's, except that CO_2 can be varied and meridional heat transport into the model domain depends on the implied meridional temperature gradient rather than being specified at a constant value.

The state variables (Table 1) are ice volume, ice area, ice surface temperature, and ocean mixed layer temperature. Their evolution is represented by four ordinary differential

Table 1: Model state variables.

V	Ice volume divided by area of box (units of m).
A	Ice area (fraction of box covered by ice).
T_i	Ice surface temperature (°C).
T_{ml}	Ocean mixed layer temperature (°C).

equations with thresholds associated with the freezing temperature of the ice surface and ocean mixed layer, as well as a threshold in the evolution of ice area associated with whether the ice volume is growing or decaying. The physical derivation of these equations is described below.

3.1 Sea ice

3.1.1 Ice thermodynamics

Here we discuss the derivation of the idealized thermodynamic equations in T92, which have been used in this model, starting from the fundamental conservation law for heat transport in a two-phase, two-component system. We discuss the equations of Maykut and Untersteiner [19] as an intermediate step.

As sea ice grows, differences in the rates of diffusion of heat and salt in seawater give rise to a region adjacent to the ice-water boundary where the water is constitutionally supercooled. This triggers morphological instability of the interface: perturbations to a planar interface grow because they protrude into the constitutionally supercooled region. Due to this effect, sea ice develops a lamellar solid-liquid interface characterized by millimeter-scale blades of ice with brine filling the narrow spaces between them. This is in contrast to the more familiar situation of lake ice, which experiences none of these salinity-related phenomena and grows with a planar solid-liquid interface.

At thermodynamic equilibrium, the interstitial brine in sea ice is at the freezing temperature, maintaining the same temperate as the ice crystals immersed in it. As explained by Maykut and Untersteiner [19], a rise in temperature causes ice crystals to melt until the brine is diluted sufficiently to raise its freezing point to the new temperature. Hence the heat capacity of a slab of sea ice is different from that of a simple solid: the brine pockets serve as a thermal reservoir, enhancing the effective heat capacity.

This suggests a treatment of sea ice in which quantities are averaged over regions containing both ice and interstitial brine. A region of mixed phase for a two-component fluid (here salt and water) is called a mushy layer. Sea ice thermodynamics can thus be described as a problem of vertical heat conduction in a mushy layer with the upper boundary condition determined by the balance of surface fluxes.

The mushy layer equation for conservation of heat can be written (Worster [36], equation 6.20)

$$c_m \frac{\partial T}{\partial t} + c_b \mathbf{u} \cdot \nabla T = \nabla \cdot (k_m \nabla T) + \mathcal{L} \frac{\partial \phi}{\partial t} + A_R \tag{1}$$

where T is the mushy layer temperature, ϕ is the solid fraction (i.e., fraction of the volume which is ice), $\mathcal{L}$ is the latent heat of fusion per unit volume (proportional to the difference in

enthalpy between brine and ice), and A_R represents the absorption of solar radiation that has passed through the surface of the ice. Here the mean volumetric specific heat capacity, $c_m = c_i\phi + c_b(1-\phi)$, is related to the volumetric specific heat of ice (c_i) and brine (c_b). The mean thermal conductively of the mushy layer is approximated to be $k_m = k_i\phi + k_b(1-\phi)$, where k_i and k_b are the thermal conductivities of pure ice and brine; this relationship is exact if the ice lamellae are oriented parallel to the heat flux, which is a good approximation for sea ice. Note that in (1) we have corrected the typographical error (verified via personal communication with Grae Worster) in the factor multiplying the advective term in Worster [36] equation 6.20.

Feltham et al [6] showed that under certain physical assumptions the mushy layer conservation equation (1) reduces to the temperature diffusion equation in the model of Maykut and Untersteiner [19], which most current models of sea ice thermodynamics are based on. Here we present a brief summary of the derivation in Feltham et al. Assuming local thermodynamic equilibrium (i.e., brine is at freezing temperature) and a linear liquidus relationship (i.e., linear dependence of brine freezing temperature, T_L, on brine salinity, S), we can relate the temperature to the brine salinity as

$$T = T_L(S) = T_L(0) - \Gamma S. \tag{2}$$

We introduce the bulk salinity, $S_{bulk} = (1-\phi)S$, using the assumption that the concentration of salt incorporated into the ice crystals is negligible compared to the brine salinity. This allows us to write the solid fraction ϕ in terms of brine salinity and hence, by (2), in terms of temperature:

$$\phi = 1 + \frac{\Gamma S_{bulk}}{\theta}. \tag{3}$$

Here we have defined $\theta \equiv T - T_L(0) = T - 273\,\mathrm{K}$.

Maykut and Untersteiner [19] use a prescribed time-independent vertical salinity profile for S_{bulk}, neglect brine flow ($\mathbf{u} = 0$), and consider temperature variations in the vertical only. Under these assumptions, (1) becomes

$$c_{\text{eff}}\frac{\partial T}{\partial t} = \frac{\partial}{\partial z}\left(k_{\text{eff}}\frac{\partial T}{\partial z}\right) + A_R. \tag{4}$$

with $c_{\text{eff}} \equiv c_m - \mathcal{L}\frac{d\phi}{d\theta}$ and $k_{\text{eff}} \equiv k_m$. Inserting (3) and the definitions of c_m and k_m, the effective mushy layer heat capacity and conductivity can be written

$$c_{\text{eff}} = c_i - \frac{\Gamma S_{bulk}}{\theta}(c_b - c_i) + \mathcal{L}\frac{\Gamma S_{bulk}}{\theta^2} \tag{5}$$

and

$$k_{\text{eff}} = k_i - \frac{\Gamma S_{bulk}}{\theta}(k_b - k_i). \tag{6}$$

Equations (5) and (6) are equivalent to Feltham et al [6] equations 14 and 15 (with their equation 14 corrected for a typographical error, verified by personal communication with Danny Feltham, in the sign of the second term).

Approximate formulas for effective heat capacity and conductivity were derived by Untersteiner [32]. Because they were found to be in good agreement with the theoretical

expressions of Schwerdtfeger [27] and Ono [24], they were used by Maykut and Untersteiner [19]. Feltham et al [6] demonstrate that sea ice heat capacity and conductivity obtained by Schwerdtfeger [27] are identical to the mushy layer result (5)-(6) when $\mathbf{L}/\rho_i$ is assumed constant, the conductivity of bubbly ice is assumed equal to k_i, the volumetric heat capacity of pure water is assumed equal to c_b, and the densities of pure water, pure ice, and sea ice are all assumed equal.

The equation in Maykut and Untersteiner [19] describing the evolution of the temperature profile (their equation 6) has capacity and conductivity terms with parameters multiplying powers of temperature and salinity in identical form to (5)-(6), with the exception that they do not have the S_{bulk}/θ term in (5). By illustrating this equivalence, Feltham et al [6] demonstrate that these terms in the thermodynamic model of Maykut and Untersteiner [19] are firmly grounded in the physics of mushy layers, thereby showing exactly how the terms account for both the fractional inclusion of brine pockets and the energy associated with phase change when this fraction evolves.

Maykut and Untersteiner [19] use a scaling argument to neglect the vertical derivative of k_{eff}, simplifying (4) to

$$c_{\text{eff}}\frac{\partial T}{\partial t} = k_{\text{eff}}\frac{\partial^2 T}{\partial z^2} + A_R. \tag{7}$$

They specify seasonally varying snowfall and include a layer of snow above the ice in which temperature evolves according to

$$c_{\text{snow}}\frac{\partial T}{\partial t} = k_{\text{snow}}\frac{\partial^2 T}{\partial z^2} + A_R. \tag{8}$$

In this layer, unlike in the mushy sea ice, the volumetric heat capacity (c_{snow}) and conductivity (k_{snow}) are constant parameters. The boundary condition at the upper surface, $z = h_T$, is a flux balance when the ice is below the freezing temperature and a Stefan condition for surface melt otherwise:

$$k_{\text{snow}}\left[\frac{\partial T}{\partial z}\right]_{h_T} - F_{top} = \begin{cases} 0 & T\left(h_T\right) < 0^o\text{C} \\ L\frac{dh_T}{dt} & T\left(h_T\right) = 0^o\text{C} \end{cases} \tag{9}$$

where L is the latent heat of fusion of the surface material and F_{top} represents the sum of sensible, latent, downward and upward longwave, and shortwave heat fluxes at the surface. All but the upward longwave flux are specified in their model based on observations. The fluxes balance at the snow-ice interface ($z = h_{si}$):

$$k_{\text{snow}}\left[\frac{\partial T}{\partial z}\right]_{h_{si}+} = \left[k_{\text{eff}}\frac{\partial T}{\partial z}\right]_{h_{si}-}. \tag{10}$$

At the base of the ice layer, $z = h_B$, a Stefan condition for ice growth or melt is applied:

$$-\left[k_{\text{eff}}\frac{\partial T}{\partial z}\right]_{h_B} - F_{bot} = -L\frac{dh_B}{dt}. \tag{11}$$

Here F_{bot} is the flux from the ocean mixed layer into the base of the ice, which is a specified constant. Note from (9) and (11) that Maykut and Untersteiner evolve the upper and lower

surfaces of the ice, h_T and h_B, separately. The actual predicted ice and snow thicknesses are $h_{\text{ice}} = h_{si} - h_B$ and $h_{\text{snow}} = h_T - h_{si}$.

The thermodynamic sea ice model of Maykut and Untersteiner [19] is summarized by (7)-(11). They solved it numerically on a 10cm vertical grid with 12 hour time steps using a $3 million 1960s IBM mainframe computer.

The simplified thermodynamic equations in T92 can be derived from (7)-(11) by neglecting snow and sensible and latent surface heat fluxes, assuming the sea ice effective heat capacity and conductivity to be independent of temperature and salinity ($c_{\text{eff}}(T,S) = c$, $k_{\text{eff}}(T,S) = k$), approximating all shortwave radiation to be absorbed at the upper surface ($A_R = 0$), and applying the quasi-stationary approximation to the diffusion equation (7). This leads to equations for the evolution of surface temperature T_i and ice thickness $h \equiv h_T - h_B$. The quasi-stationary approximation, which is based on assuming a large Stefan number $S \equiv L/(c_p \Delta T)$, allows the left hand side of (7) to be integrated with the assumption of a linear temperature profile:

$$\int_{h_B}^{h_T} dz \left(c \frac{\partial T}{\partial t} \right) = c \int_{h_B}^{h_T} dz \left(\frac{\partial}{\partial t} \left(\frac{z - h_B}{h_T - h_B} T_i \right) \right) = \frac{ch}{2} \frac{dT_i}{dt}. \tag{12}$$

This leads to an integrated version of the diffusion equation (7),

$$\frac{ch}{2} \frac{dT_i}{dt} = k \left[\frac{\partial T}{\partial z} \right]_{h_T} - k \left[\frac{\partial T}{\partial z} \right]_{h_B}. \tag{13}$$

Inserting into (13) the boundary conditions (9) and (11) leads to two sets of equations depending on whether or not the surface is melting. In either case, the linear internal temperature gradient is used for the lower boundary term ($k \left[\partial T / \partial z \right]_{h_B} = k T_i / h$) because of the Stefan condition at the edge, and the lower boundary condition (11) becomes

$$-L \frac{dh_B}{dt} = -k \frac{T_i}{h} - F_{bot}. \tag{14}$$

When $T_i < 0°\text{C}$, the first upper boundary condition in (9) gives $k \left[\partial T / \partial z \right]_{h_T} = F_{top}$. Inserting this into (13) and using $dh/dt = d/dt \left(h_T - h_B \right) = -dh_B/dt$ in (14) leads to

$$\tfrac{ch}{2} \tfrac{dT_i}{dt} = F_{top} - k T_i / h, \tag{15}$$

$$L \tfrac{dh}{dt} = -k \tfrac{T_i}{h} - F_{bot}. \tag{16}$$

When $T_i = 0°\text{C}$, the Stefan condition at the upper edge leads to the use of the internal temperature gradient for the upper boundary term, $k \left[\partial T / \partial z \right]_{h_T} = k T_i / h$. Using the second upper boundary condition in (9), $L dh_T/dt = k T_i / h - F_{top}$, (13) and (14) become

$$\tfrac{dT_i}{dt} = 0, \tag{17}$$

$$L \tfrac{dh}{dt} = -F_{top} - F_{bot}. \tag{18}$$

Thorndike [31] separates the sea ice seasonal cycle into discrete steps representing cooling, growing, warming, and melting. He uses (15)-(16) during growing and (17)-(18) during melting, and during the warming and cooling steps he uses equations to evolve T_i and h which are equivalent to letting $dh_B/dt = 0$ in the lower boundary condition (11).

In the model presented here, we use a continuously evolving seasonal cycle, using (15)-(16) or (17)-(18) depending on whether $T_i < 0°\mathrm{C}$. Because we allow partial ice cover, unlike in the models of Maykut and Untersteiner [19] and Thorndike [31], we evolve ice volume rather than ice thickness. In the ice-covered fraction of the model domain A, this vertical thermodynamic growth of the ice is represented by re-writing (16) and (18) as

$$L\frac{dV}{dt} = A\left(-k\frac{T_i}{h} - F_{bot}\right), \tag{19}$$

and

$$L\frac{dV}{dt} = A\left(-F_{top} - F_{bot}\right). \tag{20}$$

3.1.2 Evolution of ice area

T92 describes the entire Arctic by a single ice thickness, using a thermodynamic ocean mixed layer model which becomes active only when all the ice melts. In the model used here, an open water fraction is included. When the open water fraction is small, it describes the area of the Arctic covered by leads; when it is large, it describes extended regions of open water.

While the thermodynamic sea ice equations in this model are derived from fundamental physics, the area evolution is based on the observationally motivated methodology of Hibler [10]. Hibler introduced this methodology to evolve ice concentration (fraction of grid covered by ice) in each model grid box, allowing models to account for the presence of subgrid-scale leads. Many of the GCMs today with the most sophisticated sea ice representations include similar parameterizations of subgrid-scale leads and thickness distributions based on this methodology. The box model used here effectively includes a single grid box, so Hibler's methodology can be similarly applied to the ice area in this box.

It should be noted that the open water fraction in this model, as in Hibler [10] and similar models, is not meant to represent a truly ice-free region. Rather, the model domain is split into a fraction containing thick ice, with the rest covered by a mixture of exposed ocean and thin ice as in observed leads. The volume of this thin ice is assumed to be negligible compared to the thick ice volume.

Hibler [10] presents a dynamic model in which the thermodynamic sea ice growth rate is specified as a function of ice thickness and season, and concentration grows based on the growth rate for zero-thickness ice. Here the thermodynamics are computed, and concentration increases when T_{ml} reaches zero and tries to keep cooling: the mixed layer flux imbalance F_{ni} goes to making new ice volume as

$$\frac{dA}{dt} = \frac{F_{ni}}{Lh_0}. \tag{21}$$

As in Hibler, an equivalent thickness h_0 must be assigned to the new volume to give it a horizontal area. This parameter controls the rate at which ice cover grows; it is not to be viewed literally as the typical thickness of new ice.

Area grows only when the mixed layer freezes; when the Stefan condition at the ice base leads to volume growth, the ice grows vertically downward and area remains fixed.

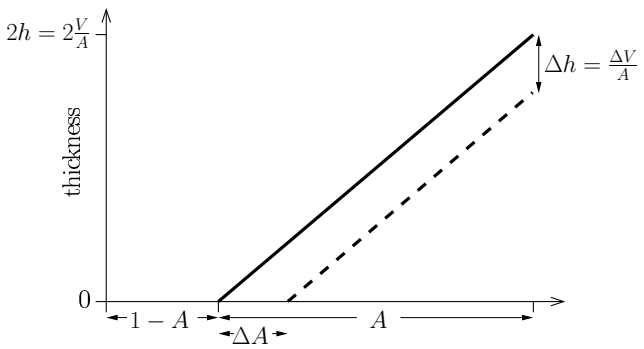

Figure 3: Schematic illustrating the proportionality between the rate of change of ice area and the thermodynamic decrease of volume. This methodology follows Hibler [10].

Area decays, however, when volume is thermodynamically lost. Following the treatment in Hibler, when $\frac{dV}{dt} < 0$ area decreases as

$$\frac{dA}{dt} = \frac{A}{2V}\frac{dV}{dt}. \tag{22}$$

The proportionality between volume and area rates of change is based on an argument in Hibler about the ice thickness distribution in the model domain. Assume that the ice is distributed evenly in thickness between 0 and $2V/A$. This gives a mean thickness of V/A. (Note, however, that in both Hibler's model and the model presented here the thermodynamic growth of ice is a nonlinear function of thickness and is computed under the assumption that all ice is of the mean thickness V/A, rather than using an even distribution between 0 and $2V/A$.) It is assumed that all ice in the 0 to $2V/A$ distribution melts at the same rate. Hence the rate of area decay is given by the rate of thickness decay times the inverse slope of the thickness distribution

$$\Delta A = \Delta h \frac{dA}{dh} = \frac{\Delta V}{A}\frac{A}{2V/A} = \frac{A}{2V}\Delta V. \tag{23}$$

This is illustrated schematically in Fig. 3.

Note that new ice area forms at $T_i = 0$, hence increasing the subzero ice surface temperature when area is expanding during the growing season. This would add the term $-(T/A)dA/dt$ to dT/dt. Since T typically changes between 0°and 30°C while A evolves between 0.75 and 1, $(1/T)dT/dt$ tends to be far larger than $(1/A)dA/dt$, and the term is expected to be insignificant and has been neglected.

Dynamics are represented in the model by requiring that $A \leq 0.95$ (because of the constant convergence and divergence of the wind field) and by imposing a net annual export of 10% of the ice area based on observations of Kwok et al [13]. The latter adds the terms $-v_0 A$ and $-v_0 V$ to the area and volume evolution equations.

3.2 Atmosphere

3.2.1 Radiative equilibrium

The model has a gray-body thermal equilibrium atmosphere, as in T92 (cf. Goody and Yung [9], Section 9.2), which is used to compute the downward longwave radiation at the surface as a function of the surface temperature. To find this relationship it is necessary to derive the full atmospheric vertical profiles of temperature and downward and upward propagating longwave radiation. The atmosphere is assumed to be transparent to shortwave (solar) radiation. A poleward atmospheric heat transport into the Arctic, D, is accounted for in the model.

With longwave extinction coefficient $\kappa(z)$ and atmospheric density $\rho(z)$, the amount of upward propagating longwave F_{UP} at a given height can be found using $dF_{UP}/dz = \rho(z)\kappa(z)F_{UP}(z)$. This can be solved for intensity as a function of height,

$$F_{UP}(z) = F_{UP}(0)\exp\left(\int_0^z \rho\kappa dz'\right) = F_{UP}(0)\exp(\eta(z)), \tag{24}$$

where $F_{UP}(0)$ is longwave radiated from the surface. Here we have defined the optical height, $\eta(z) \equiv \int_0^z \rho\kappa dz'$. An advantage of measuring height using η instead of z is that $\kappa(z)$ and $\rho(z)$ drop out of the equations and the atmosphere can be described by a single parameter, the total optical thickness $N \equiv \eta(\infty)$. Physically, an optical thickness of N means that a longwave photon typically passes through $1/N$ of the atmosphere before being absorbed.

The longwave radiation from the surface can be linearized in surface temperature, T_s, about the freezing temperature, $T_s = 0°\mathrm{C}$:

$$F_{UP}(0) = \sigma(T_s + 273K)^4 \approx a + bT_s. \tag{25}$$

Here T_s is assumed to be measured in °C.

The atmosphere is absorbing and reradiating longwave radiation at all heights. The intensity of downward radiation from the atmosphere above is given by $F_{DN}(\eta)$, which must be zero at the top of the atmosphere:

$$F_{DN}(N) = 0. \tag{26}$$

The amount of radiation absorbed by a layer of thickness $d\eta$ is $(F_{UP}(\eta) + F_{DN}(\eta))\,d\eta$. We assume the poleward heat transport is distributed evenly in optical height, so each layer gains $D/Nd\eta$ of heat from this advection. The longwave radiation from a given layer is given by $2R(\eta)d\eta$, where $R(\eta) = a + bT(\eta)$ and the factor of 2 accounts for radiation from the top and bottom of the layer. In thermodynamic equilibrium, this leads to

$$F_{UP}(\eta) + F_{DN}(\eta) + \frac{D}{N} = 2R(\eta). \tag{27}$$

The fluxes vary in height because of absorption and reradiation:

$$\frac{dF_{UP}(\eta)}{d\eta} = -F_{UP}(\eta) + R(\eta), \tag{28}$$

$$\frac{dF_{DN}(\eta)}{d\eta} = F_{DN}(\eta) - R(\eta). \tag{29}$$

Equations (27)-(29) are a system of one algebraic and two differential equations. They can be solved using the boundary conditions (25)-(26) to give R, F_{UP}, and F_{DN} at all heights η. The only part of the solution which is needed for the model is the dependence of the downward longwave radiation at the surface on surface temperature, which is found to be

$$F_{DN}(0) = (a + bT_s)\,\frac{N}{2+N} + \frac{D}{2}. \tag{30}$$

3.2.2 Seasonal cycle

The seasonal cycle in this model if forced by varying specified shortwave radiation F_{sw}, atmospheric optical thickness N, and 0–70°N temperature which is used to compute the poleward heat transport D (described in Section 3.2.3). T92 uses a step-function seasonal cycle, with summer vales of N and F_{sw} for half the year and winter values for the other half. This allows him to arrive at a closed form analytical solution to the model equations. We solve the equations numerically, and hence we can use a continually varying seasonal cycle.

Maykut and Untersteiner [19] force their model with specified shortwave forcing based on observations of solar radiation incident at the surface. The values differ significantly from the astronomically constrained top-of-the-atmosphere radiation, because the transmissivity of the Arctic atmosphere is typically only 40–70% [17]. We forced the model with a non-negative sine-wave approximation to the monthly mean data used by Maykut and Untersteiner (Fig. 4).

The optical thickness is higher during summer than winter because of increased cloudiness. T92 tuned the values of N to simulate a seasonal cycle in ice thickness similar to the more complicated model of Maykut and Untersteiner [19]; although the choice of N values was motived by matching $F_{DN}(0)$ with observed surface downward longwave flux, using summer and winter values of N which better match the cited $F_{DN}(0)$ observations (and simulated surface temperature) cause all the ice to melt in the model of T92 for any initial condition (not shown). The requirement that N be tuned to some extent is not surprising in light of the many simplifications in the model, including neglecting sensible and latent heat fluxes.

Björk and Söderkvist [2] constructed a single-column model with a sophisticated representation of the Arctic ocean, 40 evolving ice thickness categories, and an atmospheric thermal equilibrium model based on T92. They prescribed N to follow the observed annual cycle of cloudiness but tuned its magnitude to give an observationally reasonable cycle of ice thickness. We followed a similar procedure, using a non-negative sine-wave approximation to the Arctic cloudiness observations made by Maykut and Church [17] (Fig. 4). This leaves the seasonal maximum and minimum values of N as tunable constants, and we chose values to give a physically reasonable seasonal cycle in ice thickness.

3.2.3 Poleward heat transport

T92 specifies a constant poleward heat flux in the atmosphere equivalent to a vertical flux of $100\mathrm{W/m}^2$, which is based on observations [23]. He finds a state similar to the observed present-day Arctic, as well as a second stable state in which the Arctic is ice free with ocean

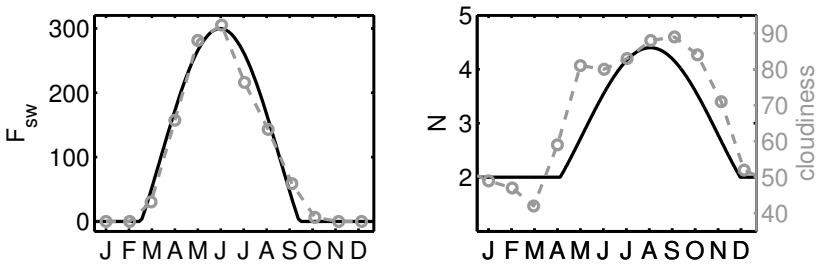

Figure 4: Seasonal cycle in specified model forcing (black lines), and observations the forcing is based on (gray circles and dashed line). (left) Shortwave radiation (W/m^2) chosen to fit observed incident solar flux at the surface [19]. (right) Optical thickness of the model atmosphere, which is scaled to match Arctic cloudiness (percent) [17].

mixed layer temperatures varying seasonally between 6° and 14°C. As mentioned in T92, it is unlikely that the real atmosphere would maintain the present-day poleward heat transport with the meridional temperature gradient significantly reduced. Thorndike later expanded on this idea, letting D be a function of the meridional temperature gradient between two boxes in a highly idealized climate model with no seasonal cycle or ice thermodynamics [30]. This method of approximating D is frequently employed in idealized atmospheric models (e.g., Chen et al [4]), and we have adopted it here.

We let

$$D(T_s) = k_D \left(T_{0-70N} - T_s\right) \tag{31}$$

with T_{0-70N} specified to vary seasonally based on NCEP-NCAR [12] observed climatological 1000mb temperature which was averaged both zonally and 0°–70°N. We used $k_D = 3.3$, equivalent to the value in Thorndike [30], which matches observed poleward heat transport [23] fairly well using T_s from the standard model run (Fig. 5). Note that when this parameterization for D is inserted into the model of T92 the ice-free states disappears, leaving only the state resembling the present-day Arctic.

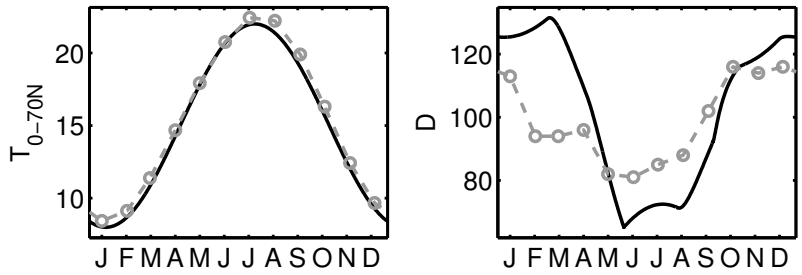

Figure 5: (left) Observed 0–70°N mean seasonal cycle in 1000mb atmospheric temperature T_{0-70N} (gray circles and dash) and a sinusoidal fit used in the model (black). (right) Observed poleward heat transport D (gray circles and dash), and computed values of D, which use T_{0-70N} and simulated Arctic surface temperature T_s, in the standard model run.

3.2.4 Surface flux exchange

The surface is split into a region containing ice and an open water region, with average surface temperature

$$T_s = AT_i + (1 - A)T_{ml}. \tag{32}$$

Surface downward longwave radiation, $F_{DN}(0)$, was computed in Section 3.2.1 using the average surface upward radiation $F_{UP}(0) = a+bT_s$. We assume that the downward longwave radiation is everywhere uniform in the model domain and depends only on T_s, but we compute the upward radiation separately for ice and open water as $F_{UP}(0) = a + bT_i$ and $F_{UP}(0) = a + bT_{ml}$ respectively. The longwave emissivities of ice and open water, both roughly 0.95 or greater, have here been approximated to 1. (Note, however, that open water and ice differ significantly in microwave emissivity, which is what satellite observing systems like SSM/I are based on.) This leads to a surface longwave radiation imbalance above ice or open water of

$$\epsilon(T, T_s) \equiv F_{UP}(0) - F_{DN}(0) = \frac{2a}{2 + N} - \frac{D(T_s)}{2} + b\left(T - T_s + \frac{2T_s}{2 + N}\right), \tag{33}$$

with $T = T_i$ or $T = T_{ml}$ inserted.

Shortwave radiation is also absorbed at the surface, adding an energy flux $(1 - \alpha)F_{sw}$ with $\alpha = \alpha_{ml}$ over open water and $\alpha = \alpha_i$ over ice. When ice is melting at the surface ($T_i = 0$), a lower albedo is used to account for the ice and the presence of melt ponds (α_{mp}). The value of α_{mp} is chosen based on observations of fractional pond cover in summer and melt pond albedos [7].

3.2.5 Addition of CO_2

We can crudely vary CO_2 in the model by enhancing the Arctic optical thickness and adjusting T_{0-70N} in the equation determining poleward heat transport. Changes in radiative forcing are typically approximated to have a logarithmic dependence on CO_2 concentration, and values associated with CO_2 doubling are commonly discussed. The IPCC TAR [11] cites a range of 1.5 to 4.5°C for the equilibrium response of an atmospheric GCM to each doubling of CO_2, so we add 3°C to T_{0-70N} for CO_2 doubling.

The IPCC TAR gives a range of 3.5-4.1 W/m^2 for the direct longwave radiative forcing due to a doubling of CO_2, suggesting 3.7 W/m^2 as the best estimate (their Section 6.3.1). Solving (30) for N, we can write the relationship between optical thickness and longwave forcing as

$$N = 2\frac{F_{DN}(0) - D/2}{a + bT_s - F_{DN}(0) + D/2}. \tag{34}$$

Replacing N with $N + \Delta N$ and replacing $F_{DN}(0)$ with $F_{DN}(0) + \Delta F$, this shows that the change in optical thickness associated with an increase in longwave forcing is

$$\Delta N = \frac{N(1 + N/2)}{F_{DN}(0) - D/2}\Delta F + O\left(\frac{\Delta F}{F_{DN}(0)}\right)^2. \tag{35}$$

We insert into (35) mean values for N, $F_{DN}(0)$, and D from the standard model run, which leads to an increase in N of $\Delta N = 0.2$ associated with the enhancement in radiative forcing of $\Delta F = 3.7$ W/m^2.

Based on this, we vary CO_2 in the model by replacing N with $N + \Delta N \log_2(co2)$ and replacing T_{0-70N} with $T_{0-70N} + \Delta T \log_2(co2)$, where $co2$ represents the factor multiplying present-day atmospheric CO_2 concentrations, $\Delta N = 0.2$, and $\Delta T = 3^o$.

3.3 Ocean mixed layer

The mixed layer is modeled as a thermodynamic reservoir. Its characteristic depth is $H_{ml} =$ 50m as in T92 (cf. observations of Morison and Smith [22]).

The flux of heat entrained through the bottom of the mixed layer is specified to be $F_{ent} = 0.5\text{W/m}^2$ based on observations [22]. The turbulent heat flux between the ocean and the base of the ice is given by $F_w = \rho c_p c_h u_{*0} \Delta T$, where ρ and c_p are the density and specific heat of seawater, $c_h = 006$ is the heat transfer coefficient, u_{*0} is the friction velocity (square root of kinematic stress at ice-ocean interface), and ΔT is the difference in temperature between ocean and ice [20]. Using a typical value of $u_{*o} = 0.5\text{cm/s}$ based on observations [18] and inserting $\Delta T = T_{ml}$ (since $T = 0$ at the base of the mixed layer) leads to

$$F_w = \gamma T_{ml} \tag{36}$$

with $\gamma \equiv \rho c_p c_h u_{*0} = 120\text{W/m}^2$.

The total heat flux into the mixed layer is thus

$$F_{ml} = (1 - A)\left(-\epsilon(T_{ml}, T_s) + (1 - \alpha_{ml})F_{sw}\right) - A\gamma T_{ml} + F_{entr}. \tag{37}$$

If $T_{ml} > 0$, this leads to heating or cooling according to

$$c_{ml} H_{ml} \frac{dT_{ml}}{dt} = F_{ml}, \tag{38}$$

and no new ice area is formed, $F_{ni} = 0$. When the mixed layer reaches the freezing temperature ($T_{ml} = 0$) and tries to keep cooling, the temperature remains at the freezing point ($dT_{ml}/dt = 0$) and any additional heat loss goes into the formation of new ice ($F_{ni} = -F_{ml}$).

3.4 Summary

The model is described schematically in Fig. 6. It consists of four coupled ODEs which are first-order and non-autonomous (F_{sw}, N, and D have time dependence). The model equations described in Sections 3.1-3.3 are summarized below.

The surface longwave radiation imbalance is

$$\epsilon(T, T_s) = \frac{2a}{2 + N} - \frac{D(T_s)}{2} + b\left(T - T_s + \frac{2T_s}{2 + N}\right) \tag{39}$$

with surface temperature $T_s = AT_i + (1 - A)T_{ml}$ and atmospheric poleward heat transport given by

$$D(T_s) = k_D\left(T_{0-70N} - T_s\right). \tag{40}$$

The mixed layer flux imbalance,

$$F_{ml} = (1 - A)\left(-\epsilon(T_{ml}, T_s) + (1 - \alpha_{ml})F_{sw}\right) - A\gamma T_{ml} + F_{entr}, \tag{41}$$

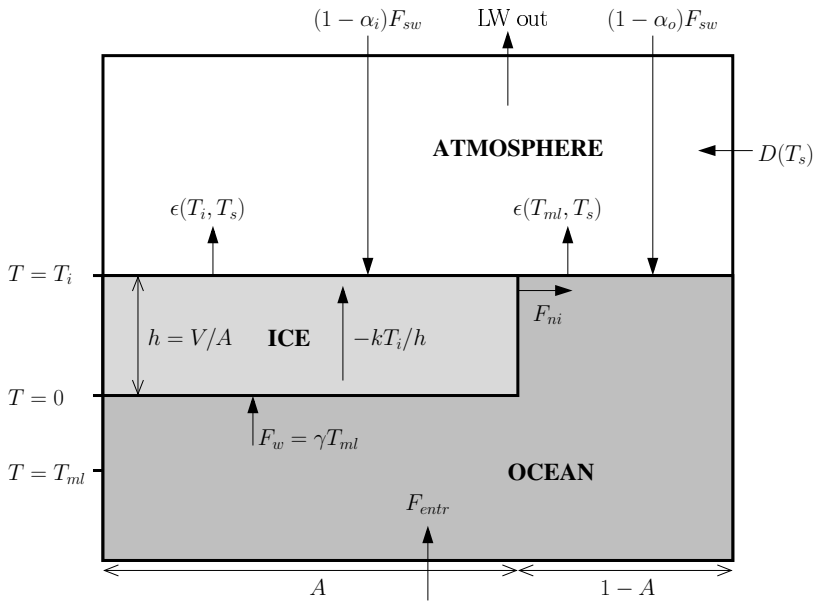

Figure 6: Schematic summarizing the model sea ice, atmosphere, and ocean thermodynamics.

normally causes warming and cooling in the mixed layer and no production of new ice area,

$$c_{ml} H_{ml} \frac{dT_{ml}}{dt} = F_{ml} \quad \text{and} \quad F_{ni} = 0. \tag{42}$$

When $T_{ml} = 0$ and $F_{ml} < 0$, however, the mixed layer flux imbalance goes into forming new ice,

$$\frac{dT_{ml}}{dt} = 0 \quad \text{and} \quad F_{ni} = -F_{ml}. \tag{43}$$

The equations for ice surface temperature and volume evolution are

$$\tfrac{ch}{2} \tfrac{dT_i}{dt} = -\epsilon(T_i, T_s) + (1-\alpha_i) F_{sw} - \tfrac{kT_i}{h}, \tag{44}$$

$$L \tfrac{dV}{dt} = A \left(-\tfrac{kT_i}{h} - \gamma T_{ml} \right) + F_{ni} - v_0 L V, \tag{45}$$

except during surface melt, $T_i = 0$ and $-\epsilon(0, T_s) + (1-\alpha_i) F_{sw} > 0$, when ice melts at the top and bottom according to

$$\tfrac{dT_i}{dt} = 0, \tag{46}$$

$$L \tfrac{dV}{dt} = A \left(\epsilon(0, T_s) - (1-\alpha_{mp}) F_{sw} - \gamma T_{ml} \right) - v_0 L V. \tag{47}$$

Here we have used the ice thickness, $h = V/A$.

The area evolves as

$$\frac{dA}{dt} = \frac{F_{ni}}{L h_0} - \frac{A}{2V} \mathcal{R} \left(-\frac{dV}{dt} \right) - v_0 A \tag{48}$$

where the ramp function $\mathcal{R}(x)$ is 0 if $x < 0$ and $\mathcal{R}(x) = x$ if $x > 0$.

The model parameters are listed in Table 2.

Table 2: Model parameters.

	Fundamental physical parameters	
c	ice heat capacity	2×10^6 J/m^3/K
L	ice latent heat of fusion	3×10^8 J/m^3
c_{ml}	mixed layer heat capacity	4×10^6 J/m^3/K
k	ice thermal conductivity	2 W/m^2/K
a	for LW radiation: $\sigma\,(T_f)^4$	320 W/m^2
b	for LW radiation: $4\sigma\,(T_f)^3$	4.6 W/m^2/K
	Parameters based closely on observations	
F_{sw}	shortwave radiation at ice or ocean surface	seasonal, 0 to 300 W/m^2
T_{0-70N}	0°–70°mean temperature	seasonal, 8 to 22°C
α_i	ice albedo	0.65
α_o	ocean albedo	0.20
α_{mp}	ice albedo during surface melt	0.55
γ	ocean–ice heat exchange coefficient	120 W/m^2/K
H_{ml}	mixed layer depth	50 m
F_{entr}	heat flux entrained into mixed layer	0.5 W/m^2
k_D	atmospheric heat transport constant	3.3 W/m^2/K
v_0	dynamic export of ice from model domain	0.10 yr^{-1}
$1 - A_{max}$	minimum lead fraction	0.05
h_0	equivalent thickness for newly formed ice	0.5 m
	Tunable parameter, based loosely on observations	
N	optical thickness	seasonal, 2 to 4.4

4 Results and discussion

The standard model run, using the parameter values in Table 2, is presented in Fig. 7. Ice thickness ($h = V/A$) varies seasonally from 2.5 to 3.7m, in rough agreement with observations. This agreement in simulated thickness extrema, while encouraging, is not surprising since we were able to tune the maximum and minimum seasonal values of N. Thickness reaches a minimum in late October and a maximum in late May, which agrees fairly well with Maykut and Untersteiner [19] who find minimum thickness in October/November and maximum thickness in June.

The ice surface temperature (T_i) varies between 0°and -32°C, and the associated trajectory in T_i versus V state space matches fairly well with the results of Maykut and Untersteiner [19] and similarly Thorndike [31].

The minimum area occurs in September, in agreement with observations. The model domain represents roughly the entire Arctic Ocean. Satellite observations [3] of the 1980-1999 mean seasonal cycle in ice extent north of 70°N (solid gray line) and 75°N (dashed gray line) are plotted next to simulated ice area for comparison. Note the fairly good agreement.

The mixed layer temperature varies between 0°and 0.23°C. When multiplied by γ, it gives the ocean–ice heat flux. The annual average flux is $F_w = 5.4$ W/m^2, which compares well with the observational estimate by Maykut and McPhee [18] of 5.1 W/m^2.

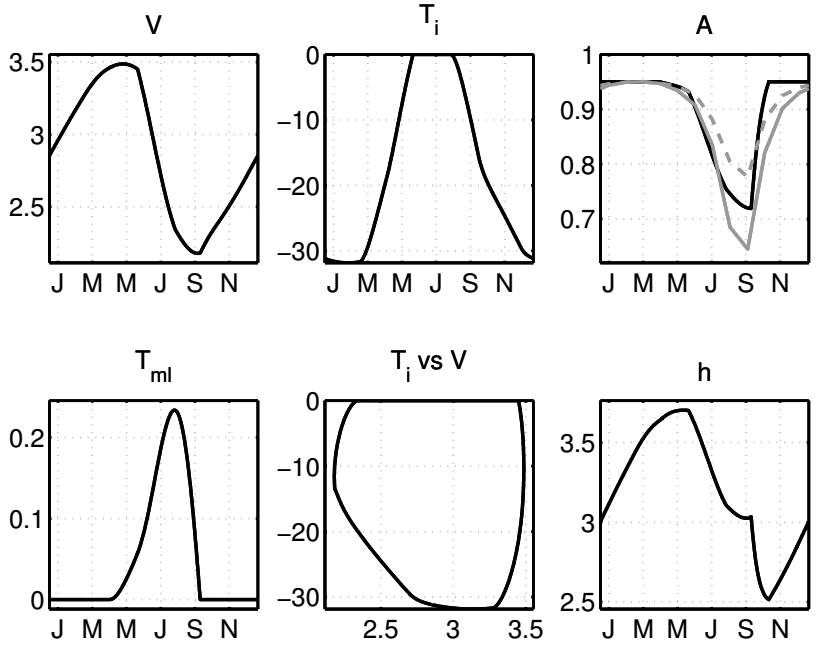

Figure 7: Standard run results. There is only one stable periodic orbit in this parameter regime, and any initial condition eventually converges on it. Plots represent evolution of the model state during the course of the annual cycle. The first four are the state variables: ice volume divided by box area V (m), ice surface temperature T_i (°C), ice area A (fraction of box covered by ice), and ocean mixed layer temperature T_{ml} (°C). The bottom center plot represents the model trajectory through the state space projected onto the T_i–V plane. The bottom right plot shows the evolution of ice thickness ($h = V/A$); note that the bump in September is related to ice area rapidly expanding while volume slowly grows, causing the average thickness to abruptly drop. Satellite observations [3] of the 1980-1999 mean seasonal cycle are included in the ice area plot for comparison; the solid gray line indicates ice extent north of 70°N and the dashed gray line indicates ice extent north of 75°N (both are plotted in units normalized to have a maximum value of 0.95).

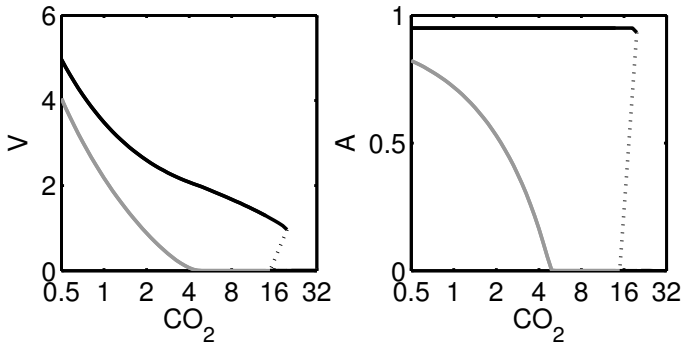

Figure 8: Response of the model solution to scaling the CO_2 parameter, which is crudely related to atmospheric CO_2 concentration. Values on the horizontal axis represent factors multiplying the CO_2 concentration today, with each tick mark representing one doubling. For each level of CO_2, the model solution is a periodic orbit in the 4-dimensional state space. Solutions are represented here by four numbers: the summer (gray) and winter (black) extrema of ice volume (left) and ice area (right). There is no hysteresis (or "tipping point") in summer ice cover. When CO_2 levels reach about $5\times$ the present-day value in this model, the Arctic becomes ice-free each summer. Further increase of CO_2 leads to multiple states and hysteresis in winter ice cover, with an associated fold catastrophe: one state has ice only in winter and the other is ice-free year-round. The multiple states exist in a narrow range on the plots around the CO_2 level of $16\times$ the present-day value. The straight dotted lines indicate the presence of an unstable state.

Varying the initial condition leads to no multiple states in the standard parameter regime: every initial condition eventually converges on the limit cycle plotted in Fig. 7. This disagrees with the "tipping point" hypothesis in which a second stable state which is ice-free each summer would exist today.

We varied CO_2, gradually raising the value and lowering it again to look for hysteresis and hence multiple states. The summer and winter extrema in ice volume and ice area are plotted in Fig. 8. A scenario in which CO_2 exponentially increases in time is equivalent to moving to the right on the horizontal axis at a constant speed: note the accelerating approach to an ice-free summer (right; gray line). However, we find no "tipping point" in summer ice cover.

When CO_2 is further increased to the point where the ocean becomes ice-free year-round, multiple states appear in a fairly narrow region of the parameter space. The region is bounded on each side by a saddle-node bifurcation of cycles where a fold catastrophe or "tipping point" occurs. Here, in an increasing CO_2 scenario, when the CO_2 level crosses a threshold the climate rapidly switches from a state characterized by nearly ice-covered winters to a state which is ice-free year-round. Note that the slight kink in the black line on the right in Fig. 8 ($CO_2 \approx 16$, $A \approx 0.95$) corresponds to a solution in which ice cover grows continuously throughout the winter and nearly fills the model domain each year before it begins to melt.

As indicated in Fig. 8, a catastrophe brought on by the demise of multiple sea ice states can occur when one state is ice-free year-round, but not when one state is ice-covered year-

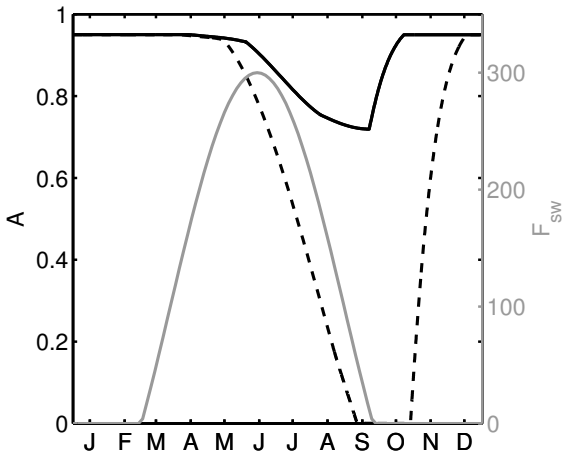

Figure 9: Simulated ice area in the standard run (black solid line) and a seasonal ice cover run with CO_2 increased by 5.3× (black dashed line), compared with solar forcing in the model (gray line; W/m^2). In the seasonal ice cover state, as in present-day observations, the minimum in ice area occurs several months after the maximum in sunlight, leading to limited overlap between significant open water and intense Arctic sunlight. This mitigates the ice–albedo effect, causing it to be outweighed by stabilizing effects and hence avoiding a "tipping point" in the approach to an ice-free summer.

round as today. As an ice-free summer is approached in an increasing CO_2 scenario, the stabilizing thermodynamic thickness–growth effect (i.e., thin ice grows fastest) appears to outweigh the destabilizing ice–albedo effect. In an attempt to understand why the heuristic argument for a "tipping point" discussed in Section 1 failed in this model for the case the present-day Arctic Ocean approaching ice-free summers, we consider why the argument seemed to succeed for the approach to an ice-free year-round state.

Fig. 9 compares the model solar forcing, which is based on Arctic surface observations (cf. Fig. 4), with simulated ice cover, which agrees fairly well with observed ice cover (cf. Fig. 7). In both the standard run (solid line) and the enhanced CO_2 seasonal ice cover solution (dashed line), there is a significant phase lag between the times of maximum sunlight and the times of minimum ice cover. This is indeed to be expected: the ice area rate of change correlates fairly well with solar intensity. For the ice–albedo effect to lead to multiple states and a catastrophe, the seasonal ice cover state must absorb significantly more sunlight than a state which is ice-covered year-round with the same parameters. But the temporal overlap in the seasonal ice state between having small ice area and experiencing a high intensity of sunlight is somewhat limited: the sun shines on a fairly extended ice cover for much of the summer. Compared to the seasonal ice state, the ice–albedo effect leads to a far bigger change when making the transition to a year-round ice-free state in which the sun shines on open water all summer.

To assess the extent to which the ice–albedo effect failed to lead to a "tipping point" in summer ice cover, we investigated whether a region exists anywhere near the physically realistic parameter regime where there are multiple summer ice cover states. We began by pushing the disparity between ice and ocean albedo to the extreme. This was not

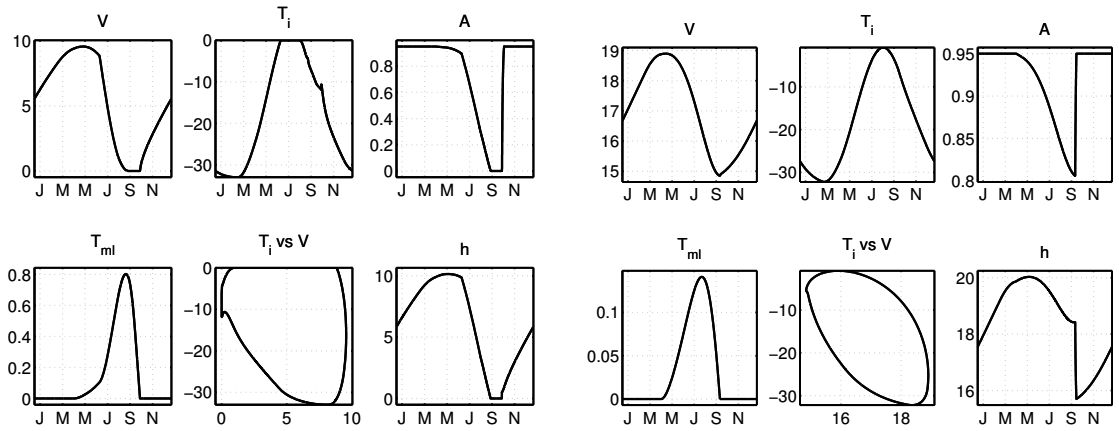

Figure 10: Multiple sea states under the same forcing. Plots represent evolution of the model variables during the seasonal cycle, as in Fig. 7, for the thin ice (left) and thick ice (right) states. Here $L^* = 10$ (i.e. sea ice latent heat of fusion is reduced $10\times$) and CO_2 has been increased to $1.5\times$ the present-day value. It should be emphasized that we are pushing the idealized model to the extremes in search of multiple summer ice states brought on by the ice–albedo effect: neither a $10\times$ diminished latent heat of fusion nor a simulated 19m ice thickness are purported here to be physically realistic.

enough to lead to multiple states. We experimented with allowing the ice albedo to depend on thickness following the parameterization of Maykut [16]. We tried varying the loosely constrained parameters. None of these approaches led to multiple summer ice cover states.

The stabilizing thickness–growth effect becomes less pronounced as ice gets thicker (i.e., very thick ice does not grow much slower than fairly thick ice), so we considered allowing excursions into state-space regions with large thickness. The most straightforward way to do this is to make it easier to grow ice by reducing the latent heat of fusion. Defining the original and observationally constrained sea ice latent heat to be L_{orig}, we scaled the latent heat according to

$$L = \frac{L_{orig}}{L^*}. \tag{49}$$

Letting $L^* = 10$ led to multiple summer ice cover states (Fig. 10).

Although the multiple states demonstrated in Fig. 10 are related to the ice–albedo effect, it should be noted that it is not the difference in albedo between open water and ice that is primarily responsible. Rather, it is the difference between the cold sea ice albedo (α_i) and the albedo used to account for the presence of melt ponds when $T_i = 0$ (α_{mp}). Both states have minimal temporal overlap between extended open water and intense sunlight, but the thin ice state has the ice surface at $T_i = 0$ for much of the peak of the summer, while in the thick ice state the surface temperature remains below the freezing temperature for the entire year.

Varying CO_2 with $L^* = 10$, we finally find the desired catastrophe (or "tipping point") in summer ice cover. This is illustrated in Fig. 11.

Next, we vary both CO_2 and L^* to explore the parameter space and find the edge of the region associated with multiple summer ice states. To do this, we slowly increase and

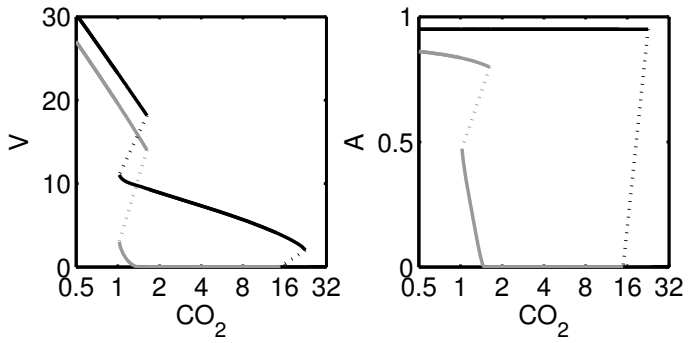

Figure 11: As in Fig. 8, by with $L^* = 10$. Now two regions exist with multiple sea ice states, and there is a catastrophe in summer ice cover (discontinuity in gray solid line).

then decrease CO_2 for an array of L^* values and look for hysteresis. The result is presented in Fig. 12. There are two regions of multiple states, each bounded by lines on which a saddle-node bifurcation of cycles occurs. These lines are associated with a cusp catastrophe: entering and then exiting either of these regions by slowly varying the parameters will lead to a catastrophe in which the current state suddenly disappears and the system rapidly approaches a new state.

Fig. 12 suggests that a catastrophe in summer ice cover would be possible if the latent heat of ice fusion were reduced from the observationally constrained value by a factor of at least 4×. The latent heat of sea ice can change depending on salinity, and observed sea ice has a salinity of roughly 0–8ppt (varying both vertically and seasonally). Theoretical and empirical formulas suggest that the latent heat of melting sea ice is about 25% lower for ice with 8ppt salinity than for pure ice (e.g., Bitz and Lipscomb [1]). The dominant variability in global mean ocean salinity over the past million years is associated with glacial cycles, during which salinity varies about the mean value of 35ppt by about 1ppt because of the reduction in ocean volume caused by the presence of large ice sheets on land. If the mean ocean salinity change associated with glacial cycles were carried into a change in mean sea ice salinity, it would lower the latent heat of fusion by 3%. This implies that a reduction in the latent heat of fusion of sea ice by 4× (i.e, 75%) would be quite significant, and it is unlikely that it could be physically realized in the foreseeable future.

5 Conclusions

We have extended Thorndike's [31] idealized Arctic sea ice model to allow for partial ice cover, adding an active ocean mixed layer and scalable CO_2. This model simulates an accelerating approach to an ice-free Arctic summer as CO_2 concentrations exponentially rise, suggesting that the approach may be fairly abrupt. We find two regions in the parameter space where multiple states are possible because of the ice–albedo effect. One region has multiple winter ice cover states (with both states ice-free in summer); the other has multiple summer ice cover states (with both states ice-covered in winter). Catastrophes are associated with exiting either region, but the actual Arctic appears to be far from the region in

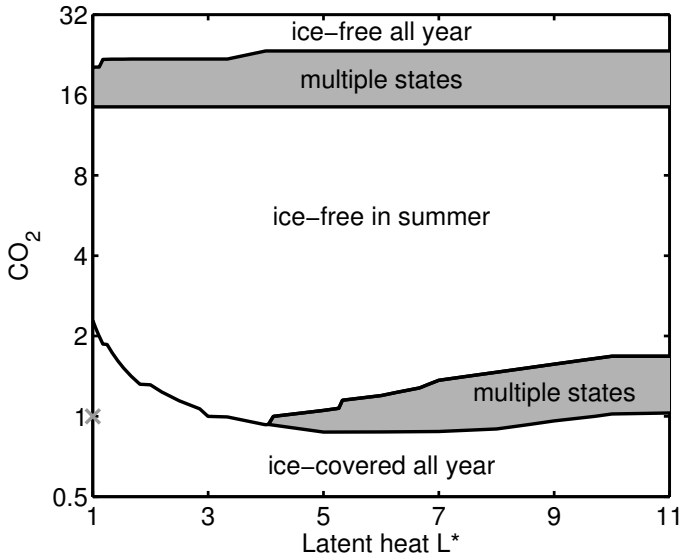

Figure 12: Regions where multiple states are possible in CO_2 versus latent heat parameter space. A saddle-node bifurcation of cycles associated with a cusp catastrophe occurs at the edge of each shaded region. Inside each shaded region there are three possible solutions: two stable periodic orbits and one unstable periodic orbit. The gray "x" marks the present-day physical world. This implies that for a "tipping point" in summer ice cover to be possible, the latent heat of sea ice fusion would have to be $4\times$ smaller than it is in the present-day physical world ($L^* = 4$). This model does find a "tipping point" in the distant but physically realizable parameter space ($L^* = 1$, $CO_2 = 20\times$ present-day) associated with the transition from seasonal ice cover to a state which is ice-free all year.

parameter space where CO_2 changes could cause a catastrophe in summer ice cover.

This research suggests that a "tipping point" in summer Arctic sea ice cover brought on by the ice–albedo affect, which has been conjectured to be likely for the 21st century, does not occur in a physically realistic region of the parameter space. In light of the fact that the seasonal minimum in ice cover occurs several months after the time of maximum Arctic sunlight, the destabilizing ice–albedo effect is not sufficient to outweigh the stabilizing thickness–growth effect and produce multiple summer sea ice states.

This model is a significantly idealized representation of the physical world. Similar to Thorndike [31], the model does not include ridging, snow, sensible and latent heat exchange, salinity, or cloud feedbacks. It is possible that other bifurcations would be introduced by adding more realistic physics to the model. For example, a wide variety of parameterizations of sea ice albedo variations have been presented in previous studies (e.g., Maykut [16], Flato and Brown [8]) and may affect these results. Furthermore, despite our fairly thorough investigations, other bifurcations may be hiding nearby in the ~ 20-dimensional parameter space.

Nonetheless, all the physics in the standard argument for a "tipping point" brought on by ice albedo has been faithfully represented in this model. This result suggests that the popular heuristic may not hold up when properly quantified.

Acknowledgments

This work benefited significantly from discussions with many visitors and staff at the GFD summer program. I am particularly grateful to John Wettlaufer who supervised the summer project, as well as Norbert Untersteiner, John Walsh, Jamie Morison, Dick Moritz, Danny Feltham, Göran Björk, Bert Rudels, Doug Martinson, Andrew Fowler, George Veronis, and Victor Tsai. I would also like to thank Alan Thorndike, who's 1992 paper formed the foundation for this model, for a helpful phone meeting in August. This work drew upon research carried out during the spring with Eli Tziperman, and I am grateful for his advising and also for helpful conversations with Cecilia Bitz during that time. Lastly, I would like to thank the other GFD fellows and staff for a great summer.

The IPCC AR4 data was downloaded from `https://esg.llnl.gov:8443`. I appreciate the 16 modeling groups for making their data available and the Program for Climate Model Diagnostics and Intercomparison at Lawrence Livermore National Laboratory for compiling the data and allowing me access to it for this project. NCEP-NCAR Reanalysis data was provided by the NOAA/OAR/ESRL PSD website.

References

[1] C. M. Bitz and W. H. Lipscomb, *An energy-conserving thermodynamic model of sea ice*, Journal of Geophysical Research-oceans, 104 (1999), pp. 15669–15677.

[2] G. Bjork and J. Soderkvist, *Dependence of the Arctic Ocean ice thickness distribution on the poleward energy flux in the atmosphere*, Journal of Geophysical Research-oceans, 107 (2002).

[3] D. Cavalieri, C. Parkinson, P. Gloerson, and H. Zwally, *Sea ice concentrations from Nimbus-7 SSMR and DMSP SSM/I passive microwave data*, Boulder, CO, USA: National Snow and Ice Data Center, (1997, updated 2005).

[4] D. Chen, R. Gerdes, and G. Lohmann, *A 1-D atmospheric energy-balance model developed for ocean modeling*, Theoretical and Applied Climatology, 51 (1995), pp. 25–38.

[5] M. Ewing and W. L. Donn, *A theory of ice ages*, Science, 123 (1956), pp. 1061–1066.

[6] D. L. Feltham, N. Untersteiner, J. S. Wettlaufer, and M. G. Worster, *Sea ice is a mushy layer*, Geophysical Research Letters, 33 (2006).

[7] F. Fetterer and N. Untersteiner, *Observations of melt ponds on Arctic sea ice*, Journal of Geophysical Research-oceans, 103 (1998), pp. 24821–24835.

[8] G. M. Flato and R. D. Brown, *Variability and climate sensitivity of landfast Arctic sea ice*, Journal of Geophysical Research-oceans, 101 (1996), pp. 25767–25777.

[9] R. Goody and Y. Yung, *Atmospheric Radiation: Theoretical Basis*, Oxford University Press, 2 ed., 1989.

[10] W. D. Hibler, *A dynamic thermodynamic sea ice model*, J. Phys. Oceanogr., 9 (1979), pp. 815–846.

[11] J. T. Houghton, Y. Ding, D. Griggs, M. Noguer, P. J. van der Linden, and D. Xiaosu, eds., *IPCC third assessment report: Climate change 2001: The scientific basis*, Cambridge University Press, Cambridge, UK, 944pp, 2001.

[12] E. Kalnay, M. Kanamitsu, R. Kistler, W. Collins, D. Deaven, L. Gandin, M. Iredell, S. Saha, G. White, J. Woollen, Y. Zhu, M. Chelliah, W. Ebisuzaki, W. Higgins, J. Janowiak, K. C. Mo, C. Ropelewski, J. Wang, A. Leetmaa, R. Reynolds, R. Jenne, and D. Joseph, *The NCEP/NCAR 40-year reanalysis project*, Bulletin of the American Meteorological Society, 77 (1996), pp. 437–471.

[13] R. Kwok, G. F. Cunningham, and S. S. Pang, *Fram strait sea ice outflow*, Journal of Geophysical Research-oceans, 109 (2004).

[14] R. W. Lindsay and J. Zhang, *The thinning of Arctic sea ice, 1988-2003: Have we passed a tipping point?*, Journal of Climate, 18 (2005), pp. 4879–4894.

[15] S. Manabe and R. J. Stouffer, *Co2-climate sensitivity study with a mathematical-model of the global climate*, Nature, 282 (1979), pp. 491–493.

[16] G. A. Maykut, *Large-scale heat-exchange and ice production in the central Arctic*, Journal of Geophysical Research-oceans and Atmospheres, 87 (1982), pp. 7971–7984.

[17] G. A. Maykut and P. E. Church, *Radiation climate of Barrow, Alaska, 1962-66*, Journal of Applied Meteorology, 12 (1973), pp. 620–628.

[18] G. A. Maykut and M. G. Mcphee, *Solar heating of the Arctic mixed layer*, Journal of Geophysical Research-oceans, 100 (1995), pp. 24691–24703.

[19] G. A. Maykut and N. Untersteiner, *Some results from a time-dependent thermodynamic model of sea ice*, J. Geophys. Res., 76 (1971), pp. 1550–1575.

[20] M. G. Mcphee, *Turbulent heat-flux in the upper ocean under sea ice*, Journal of Geophysical Research-oceans, 97 (1992), pp. 5365–5379.

[21] K. Moran, J. Backman, H. Brinkhuis, S. C. Clemens, T. Cronin, G. R. Dickens, F. Eynaud, J. Gattacceca, M. Jakobsson, R. W. Jordan, M. Kaminski, J. King, N. Koc, A. Krylov, N. Martinez, J. Matthiessen, D. Mcinroy, T. C. Moore, J. Onodera, M. O'regan, H. Palike, B. Rea, D. Rio, T. Sakamoto, D. C. Smith, R. Stein, K. St john, I. Suto, N. Suzuki, K. Takahashi, M. Watanabe, M. Yamamoto, J. Farrell, M. Frank, P. Kubik, W. Jokat, and Y. Kristoffersen, *The Cenozoic palaeoenvironment of the Arctic ocean*, Nature, 441 (2006), pp. 601–605.

[22] J. Morison and J. D. Smith, *Seasonal-variations in the upper Arctic ocean as observed at T-3*, Geophysical Research Letters, 8 (1981), pp. 753–756.

[23] N. Nakamura and A. H. Oort, *Atmospheric heat budgets of the polar-regions*, Journal of Geophysical Research-atmospheres, 93 (1988), pp. 9510–9524.

[24] N. Ono, *Physics of Snow and Ice*, vol. 1, Inst. of Low Temp. Sci., Hokkaido, Japan, 1967, ch. Specific heat and heat of fusion of sea ice, pp. 599–610.

[25] J. Overpeck, M. Sturm, J. A. Francis, D. K. Perovich, M. C. Serreze, R. Benner, E. C. Carmack, F. S. C. III, S. C. Gerlach, L. C. Hamilton, L. D. Hinzman, M. Holland, H. P. Huntington, J. R. Key, A. H. Lloyd, G. M. MacDonald, J. McFadden, D. Noone, T. D. Prowse, P. Schlosser, and C. Vvrvsmarty, *Arctic system on trajectory to new, seasonally ice-free state*, EOS, 86 (2005), pp. 309–313.

[26] C. L. Parkinson, K. Y. Vinnikov, and D. J. Cavalieri, *Evaluation of the simulation of the annual cycle of Arctic and Antarctic sea ice coverages by 11 major global climate models*, Journal of Geophysical Research-oceans, 111 (2006).

[27] P. Schwerdtfeger, *The thermal properties of sea ice*, J. Glaciol., 4 (1963), pp. 789–807.

[28] M. C. Serreze and J. A. Francis, *The Arctic amplification debate*, Climatic Change, 76 (2006), pp. 241–264.

[29] J. C. Stroeve, M. C. Serreze, F. Fetterer, T. Arbetter, W. Meier, J. Maslanik, and K. Knowles, *Tracking the Arctic's shrinking ice cover: Another extreme September minimum in 2004*, Geophysical Research Letters, 32 (2005).

[30] A. Thorndike, *A minimal model of sea ice and climate*, in Ice Physics and the Natural Environment, N. U. J.S. Wettlaufer, J.G. Dash, ed., Springer-Verlag, 1999, pp. 169–183.

[31] A. S. Thorndike, *A toy model linking atmospheric thermal radiation and sea ice growth*, J. Geophys. Res., 97 (1992), pp. 9401–9410.

[32] N. Untersteiner, *On the mass and heat budget of Arctic sea ice*, Arch. Meteorol. Geophys. Bioklimatol., Ser. A, 12 (1961), pp. 151–181.

[33] ——, *Ice budget of the Arctic ocean*, in Proceedings of the Arctic Basin Symposium, 1963, pp. 219–230.

[34] G. Walker, *The tipping point of the iceberg*, Nature, 441 (2006), pp. 802–805.

[35] J. E. Walsh, *Climate change: The Arctic as a bellwether*, Nature, 352 (1991), pp. 19–20.

[36] M. Worster, *Perspectives in Fluid Dynamics*, Cambridge University Press, 2000, ch. Solidification of fluids, pp. 393–446.